Analysis of Core-Mode to Radiation-Mode Coupling in Fiber Bragg Gratings with Finite Cladding Radius

Yahei Koyamada, *Member, IEEE*

***Abstract*—Fiber Bragg gratings (FBGs) are often surrounded with dielectric material whose refractive index is higher than that of cladding. The purpose is to prevent cladding modes because coupling to cladding modes may cause undesirable dips on the short wavelength side of the main Bragg band in the core-mode transmission spectrum. In such FBGs, core-mode to radiation-mode coupling can cause a loss band continuum. Until now, however, reported analyses of this core-mode to radiation-mode coupling have been limited to hypothetical FBGs with an infinite cladding radius. This paper presents, to the best of our knowledge, the first analysis of core-mode to radiation-mode coupling in real FBGs with a finite cladding radius. We derive a formula to calculate the core-mode transmission loss caused by the radiation-mode coupling. We show calculated core-mode transmission spectra that exhibit such fringes as have already been observed experimentally but not yet theoretically estimated.**

***Index Terms*—Cladding mode, fiber Bragg gratings (FBGs), mode coupling, radiation loss, radiation mode.**

I. Introduction

OPTICAL fiber gratings have attracted much attention in recent years due to their numerous applications in fiber-optic communication and sensor systems [1]. Short period fiber gratings, called fiber Bragg gratings (FBGs), have been used as, for example, narrow band rejection filters, add–drop filters, dispersion compensators, and sensors. However, in an FBG with a photosensitive core, the guided core mode (LP_{01} mode) not only reflects into the core mode itself but also into the cladding modes or radiation modes. This coupling causes a series of loss bands on the short wavelength side of the main Bragg band in the core-mode transmission spectrum. This loss can be quite severe in strong gratings and restricts the use of these gratings in WDM systems.

The way in which light is coupled out of the core mode depends on the refractive index of the dielectric material that surrounds the FBG [2]. If the index of the surrounding material is lower than that of the cladding, the fiber supports cladding modes that are bound modes of the total fiber. In this case, the core mode couples with the cladding modes. In contrast, when the index is higher in the surrounding material than in the cladding, the fiber does not support any cladding modes and the core mode couples with the radiation modes.

There have been many studies on the coupling of the core mode to the cladding modes including theoretical analysis [3]. On the other hand, there have been few reports on coupling to the radiation modes. Theoretical analysis has been undertaken only for hypothetical FBGs with an infinite cladding radius [4].

This paper presents, to the best of our knowledge, the first analysis of the coupling of the core mode to the radiation modes in real FBGs that have a finite cladding radius and are surrounded by dielectric material whose refractive index can differ from that of the cladding. Although, we focus on axially symmetrical FBGs, the results can easily be extended to asymmetrical FBGs [5]. The remainder of this paper is organized as follows. In Section II, radiation mode field distributions are given for fibers with a finite cladding radius. We apply coupled mode theory to our problem in Section III, and Section IV provides some numerically calculated results on the transmission spectra through the FBGs. Our conclusions are presented in Section V.

II. Radiation Modes of Fibers with Finite Cladding Radius

The electromagnetic field of the radiation modes was described by Marcuse [6] for fibers with an infinite cladding radius. Here, we extend it to fibers that have a finite cladding radius and are surrounded by dielectric material. The profile of the refractive index in the fiber and the surrounding material is shown in Fig. 1.

Here we consider the axially symmetrical radiation modes since the bound core LP_{01} mode only couples with the symmetrical modes in symmetrical FBGs. By using the weakly guiding approximation, we obtained the linearly polarized transverse electromagnetic field of the symmetrical radiation modes as follows:

$$\vec{E}_\xi(r,\, z,\, t) = F_\xi(r) \exp\, j(\omega t - \beta_\xi z)\vec{e}_e \tag{1}$$

$$\vec{H}_\xi(r,\, z,\, t) = n\sqrt{\frac{\varepsilon_0}{\mu_0}}\, F_\xi(r) \exp\, j(\omega t - \beta_\xi z)\vec{e}_h \tag{2}$$

with

$$\begin{aligned} F_\xi(r) &= A_\xi J_0(\sigma r) \qquad (r \le a) \\ &= A_\xi U_0(\rho r) \qquad (a < r \le b) \\ &= A_\xi V_0(\xi r) \qquad (b < r) \end{aligned} \tag{3}$$

where

$\vec{e}_e$ and $\vec{e}_h$	unit vectors normal to the fiber axis and to each other;
z	position along the fiber axis;
r	radial position;
a and b	radii of the core and the cladding;
$J_0(\sigma r)$	Bessel function.

Manuscript received April 4, 2000.

The author is with the Department of Media and Telecommunications Engineering, Ibaraki University, Ibaraki 316-8511, Japan.

Publisher Item Identifier S 0733-8724(00)08079-8.

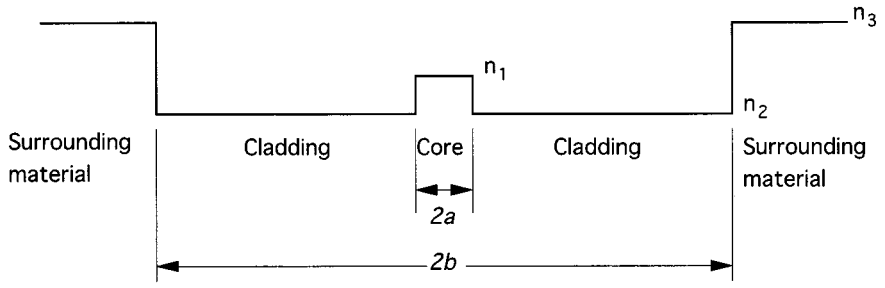

Fig. 1. Radial distribution of the refractive index in the fiber and surrounding material.

$U_0(\rho r)$ and $V_0(\xi r)$ are the functions defined by

$$U_0(\rho r) = BH_0^{(1)}(\rho r) + CH_0^{(2)}(\rho r) \tag{4}$$

$$V_0(\xi r) = DH_0^{(1)}(\xi r) + EH_0^{(2)}(\xi r) \tag{5}$$

and where $H_0^{(1)}(\sigma r)$, $H_0^{(2)}(\sigma r)$, $H_0^{(1)}(\xi r)$, $H_0^{(2)}(\xi r)$ are the Hankel functions and B, C, D, E, σ, ρ, and ξ are constants given by

$$B = j\frac{\pi a}{4}\left\{\sigma J_1(\sigma a)H_0^{(2)}(\rho a) - \rho J_0(\sigma a)H_1^{(2)}(\rho a)\right\} \tag{6}$$

$$C = -j\frac{\pi a}{4}\left\{\sigma J_1(\sigma a)H_0^{(1)}(\rho a) - \rho J_0(\sigma a)H_1^{(1)}(\rho a)\right\} \tag{7}$$

$$D = j\frac{\pi b}{4}\left\{\rho U_1(\rho b)H_0^{(2)}(\xi b) - \xi U_0(\rho b)H_1^{(2)}(\xi b)\right\} \tag{8}$$

$$E = -j\frac{\pi b}{4}\left\{\rho U_1(\rho b)H_0^{(1)}(\xi b) - \xi U_0(\rho b)H_1^{(1)}(\xi b)\right\} \tag{9}$$

$$\sigma = \sqrt{n_1^2k^2 - \beta_\xi^2} \tag{10}$$

$$\rho = \sqrt{n_2^2k^2 - \beta_\xi^2} \tag{11}$$

$$\xi = \sqrt{n_3^2k - \beta_\xi^2}. \tag{12}$$

Here n_1, n_2, and n_3 are the refractive indexes of the core, cladding, and surrounding material, respectively, and $k = \omega/c$, where ω is angular frequency and c is the velocity of light in a vacuum. The subscript ξ is used to distinguish radiation modes that differ in the radial wave number ξ in the surrounding material. Equations (6) and (7) were derived in [6] from the boundary condition whereby $F_\xi(r)$ and $dF_\xi(r)/dr$ are continuous at the core-cladding interface ($r = a$), and we have derived (8) and (9) from the same condition at the cladding-surrounding interface ($r = b$).

Equations (4) and (5) can be modified into combinations of the Bessel and Nuemann functions as

$$U_0(\rho r) = B'J_0(\rho r) + C'N_0(\rho r) \tag{13}$$

$$V_0(\xi r) = D'J_0(\xi r) + E'N_0(\xi r) \tag{14}$$

where B', C', D', and E' are constants given by

$$B' = \frac{\pi a}{2}\{\sigma J_1(\sigma a)N_0(\rho a) - \rho J_0(\sigma a)N_1(\rho a)\} \tag{15}$$

$$C' = -\frac{\pi a}{2}\{\sigma J_1(\sigma a)J_0(\rho a) - \rho J_0(\sigma a)J_1(\rho a)\} \tag{16}$$

$$D' = \frac{\pi b}{2}\{\rho U_1(\rho b)N_0(\xi b) - \xi U_0(\rho b)N_1(\xi b)\} \tag{17}$$

$$E' = -\frac{\pi b}{2}\{\rho U_1(\rho b)J_0(\xi b) - \xi U_0(\rho b)J_1(\xi b)\}. \tag{18}$$

The following orthogonality relation can be derived with the help of the weakly guiding approximation and the asymptotic forms of the Hankel functions for large values of the arguments:

$$\tfrac{1}{2}\int_0^{2\pi} d\phi \int_0^{\infty} r\left[\vec{E}_\xi \times \vec{H}_{\xi'}^*\right]_z dr = P_\xi \delta(\xi - \xi') \tag{19}$$

with

$$P_\xi = \frac{4\pi n^2 k \cdot DE}{\beta_\xi \xi}\sqrt{\frac{\varepsilon_0}{\mu_0}}A_\xi^2 \tag{20}$$

where $\delta(\xi - \xi')$ is the Dirac delta function. P_ξ is an important parameter that relates to the power carried by a continuum of radiation modes and is used in the coupled mode theory, as described in the next section.

Fig. 2 shows calculated field distributions $F_\xi(r)$ for cross sections of fibers that have a core radius of $a = 2.3\,\mu$m and a cladding radius of $b = 62.5\,\mu$m and are surrounded with (a) index-matching material ($n_3 = n_2$) and (b), (c) high index material ($n_3 = 1.01n_2$). Here, Fig. 2(b) is for the β_ξ value at which $F_\xi(r)$ is maximum at the cladding-surrounding interface ($r = b$), whereas Fig. 2(c) is for the β_ξ value where $F_\xi(r)$ becomes zero at $r = b$. The index-matching surrounding material simulates an infinite cladding. In Fig. 2(a), away from the origin, the field varies almost sinusoidally in the radial direction with decreasing magnitude. This is understood by noting that, for large values of the arguments, the Bessel and Neumann functions included in (13) and (14) approach sinusoids divided by the square root of the arguments. From Fig. 2(b) and (c), we can see that the electromagnetic field of the radiation modes is influenced significantly by the index mismatch between the cladding and surrounding material, even if the degree of mismatch is small. The effect is such that the period of radial variation becomes shorter in the surrounding material ($r > b$), because the radial wavenumber ξ in the surrounding material is larger than that ρ in the cladding. In addition, in Fig. 2(c), the field magnitude drops significantly at the cladding-surrounding interface. This is due to destructive interference resulting from the partial reflection at the cladding-surrounding interface. By

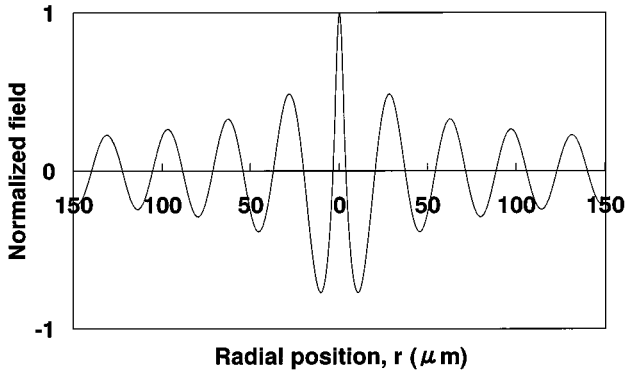

(a)

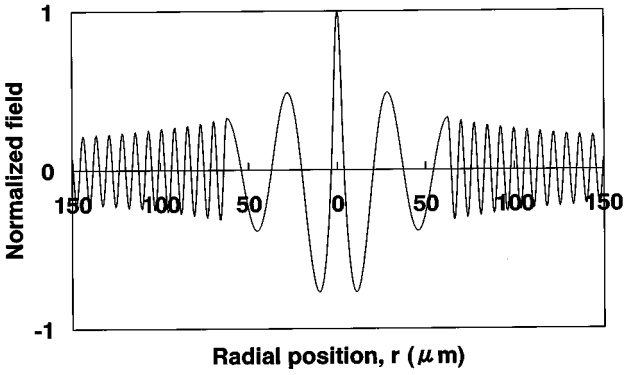

(b)

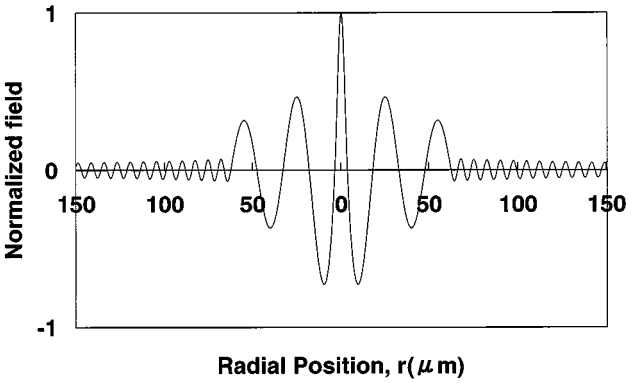

(c)

Fig. 2. Calculated field distributions of the radiation modes for fibers surrounded with (a) index-matching material ($n_3 = n_2$) and (b), (c) high index material ($n_3 = 1.01n_2$). Here (b) is for the β_ξ value at which $F_\xi(r)$ is maximum at the cladding-surrounding interface ($r = b$), whereas (c) is for the β_ξ value at which $F_\xi(r)$ becomes zero at $r = b$.

referring to Fig. 2(b) and (c), we know that the magnitude of the field in the surrounding material depends on the $F_\xi(r)$ value at the cladding-surrounding interface ($r = b$). Since the value of $F_\xi(b)$ varies periodically with β_ξ, we can expect that the magnitude of the field in the surrounding material will vary periodically with β_ξ.

We describe the electromagnetic field of the bound core LP_{01} mode as follows [6] for use in the next section:

$$\vec{E}_c(r, z, t) = F_c(r) \exp\, j(\omega t - \beta_c z)\vec{e}_e \tag{21}$$

$$\vec{H}_c(r, z, t) = n\sqrt{\frac{\varepsilon_0}{\mu_0}}\, F_c(r) \exp\, j(\omega t - \beta_c z)\vec{e}_h \tag{22}$$

with

$$F_c(r) = A_c J_0(\kappa r) \qquad (r \le a)$$
$$= A_c \frac{J_0(\kappa a)}{K_0(\gamma a)} K_0(\gamma r) \qquad (a < r) \tag{23}$$

where $K_0(\gamma r)$ is the modified Bessel function, and κ and γ are given by

$$\kappa = \sqrt{n_1^2 k^2 - \beta_c^2} \tag{24}$$

$$\gamma = \sqrt{\beta_c^2 - n_2^2 k^2}. \tag{25}$$

The power carried by the LP_{01} mode is given by

$$P_c = \tfrac{1}{2} \int_0^{2\pi} d\phi \int_0^{\infty} r \left[\vec{E}_c \times \vec{H}_c^*\right]_z dr$$
$$= \frac{\pi a^2 n (n_1^2 - n_2^2) k^2 J_1^2(\kappa a)}{2\gamma^2} \sqrt{\frac{\varepsilon_0}{\mu_0}}\, A_c^2. \tag{26}$$

III. Coupled Mode Theory Applied to Core-Mode and Radiation-Modes Within FBGs

A fiber grating is a periodic perturbation to the refractive index along the length of a fiber which is induced by exposing the fiber core to a spatially varying pattern of ultraviolet intensity. Here we assume a refractive index in the core described by

$$n(z) = n_1 + \Delta n \left\{1 + m \cos\left(\frac{2\pi}{\Lambda} z\right)\right\} \tag{27}$$

where

- Δn index change spatially averaged over the grating period;
- m fringe visibility of the index change;
- λ grating period.

The second term in (27) is the "dc" perturbation that causes a slight change in the propagation constants and field distributions of the bound core and radiation modes, respectively, but does not cause coupling between the progressive and regressive modes. The third term is the "ac" perturbation that causes coupling between the progressive and regressive modes.

In order to analyze FBGs, we first derive the LP_{01} and radiation modes for a fiber with "dc" perturbation but without "ac" perturbation. They are given by the equations found in the previous section, with n_1 replaced by $n_1 + \Delta n$. Next, we express the transverse electromagnetic field in the FBG as a superposition of the LP_{01} mode and the radiation modes of the fiber with "dc" perturbation

$$\vec{E}(r, z, t) = c_{c+}(z)\vec{E}_{c+}(r, z, t) + c_{c-}(z)\vec{E}_{c-}(r, z, t)$$
$$+ \int \left\{c_{\xi+}(z)\vec{E}_{\xi+}(r, z, t) + c_{\xi-}(z)\vec{E}_{\xi-}(r, z, t)\right\} d\xi \tag{28}$$

$$\vec{H}(r, z, t) = c_{c+}(z)\vec{H}_{c+}(r, z, t) - c_{c-}(z)\vec{H}_{c-}(r, z, t)$$
$$+ \int \left\{c_{\xi+}(z)\vec{H}_{\xi+}(r, z, t) - c_{\xi-}(z)\vec{H}_{\xi-}(r, z, t)\right\} d\xi \tag{29}$$

where $c_{c+}(z)$, $c_{c-}(z)$, $c_{\xi+}(z)$ and $c_{\xi-}(z)$ are slowly varying amplitudes of the progressive LP_{01} mode, regressive LP_{01} mode, progressive radiation modes, and regressive radiation modes, respectively. The presence of an "ac" perturbation causes the modes to be coupled with the modes traveling in the opposite direction. At the wavelengths where $2\beta_c \approx 2\pi/\Lambda$ holds, there is strong coupling between the progressive and regressive LP_{01} modes creating a main Bragg band, which is not described in detail here. On the short wavelength side of the main Bragg band where $\beta_c + \beta_\xi \approx 2\pi/\Lambda$ holds, coupling of the progressive LP_{01} mode to the regressive radiation modes becomes noticeable. In this case, the following coupled mode equations are found by substituting (27)–(29) in the Maxwell equations and neglecting terms that contain a rapidly oscillating z dependence [6]

$$\frac{dc_{c+}(z)}{dz} = -j \int g_{c\xi} \exp(j\phi_{c\xi} z) c_{\xi-}(z)\, d\xi \tag{30}$$

$$\frac{dc_{\xi-}(z)}{dz} = j g_{\xi c} \exp(-j\phi_{c\xi} z) c_{c+}(z) \tag{31}$$

where

$$\phi_{c\xi} = \beta_c + \beta_\xi - \frac{2\pi}{\Lambda} \tag{32}$$

$$g_{ij} = m\Delta n h_{ij} \qquad (i, j = c, \xi) \tag{33}$$

with

$$h_{ij} = \frac{\omega\varepsilon_0}{4P_i} \int_0^{2\pi} d\phi \int_0^a n_1 F_i(r) F_j(r) r\, dr \qquad (i, j = c, \xi). \tag{34}$$

Since (30) and (31) are difficult to solve directly, we solve them approximately by expanding $c_{c+}(z)$ and $c_{\xi-}(z)$ in a Taylor series of $\eta = m\Delta n$

$$c_{c+}(z) = c_{c+}^{(0)}(z) + \eta c_{c+}^{(1)}(z) + \eta^2 c_{c+}^{(2)}(z) + \eta^3 c_{c+}^{(3)}(z) + \cdots \tag{35}$$

$$c_{\xi-}(z) = c_{\xi-}^{(0)}(z) + \eta c_{\xi-}^{(1)}(z) + \eta^2 c_{\xi-}^{(2)}(z) + \eta^3 c_{\xi-}^{(3)}(z) + \cdots. \tag{36}$$

Substituting (35) and (36) into (30) and (31) and equating terms with the same η dependence, we find

$$\frac{d}{dz} c_{c+}^{(0)}(z) = \frac{d}{dz} c_{\xi-}^{(0)}(z) = 0 \tag{37}$$

$$\frac{dc_{c+}^{(n)}(z)}{dz} = -j \int h_{c\xi} \exp(j\phi_{c\xi} z) c_{\xi-}^{(n-1)}(z)\, d\xi \cdot (n \geq 1) \tag{38}$$

$$\frac{dc_{\xi-}^{(n)}(z)}{dz} = j h_{\xi c} \exp(-j\phi_{c\xi} z) c_{c+}^{(n-1)}(z) \qquad (n \geq 1). \tag{39}$$

From (37) we obtain $c_{c+}^{(0)}(z) = \text{const.}$ and $c_{\xi-}^{(0)}(z) = \text{const.}$ For $n \geq 1$, $c_{c+}^{(n)}(z)$ and $c_{\xi-}^{(n)}(z)$ can be determined from

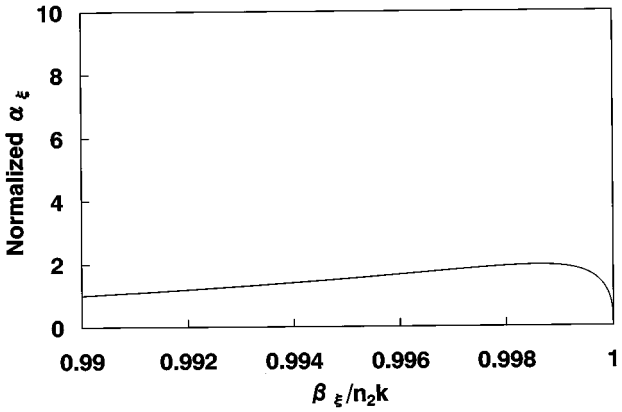

(a)

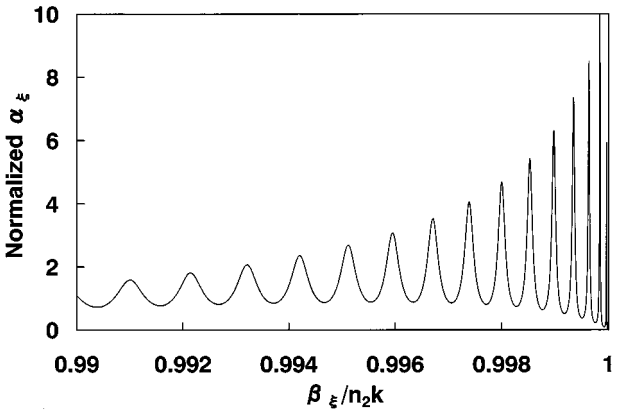

(b)

Fig. 3. The factor α_ξ as a function of β_ξ for FBGs surrounded with (a) index-matching material ($n_3 = n_2$) and (b) high index material ($n_3 = 1.01 n_2$).

$c_{\xi-}^{(n-1)}(z)$ and $c_{c+}^{(n-1)}(z)$ by using (38) and (39) successively. Under boundary conditions whereby $c_{c+}(0) = c_0$ and $c_{\xi-}(L) = 0$, where L denotes the length of the grating, $c_{c+}(z)$ is approximately obtained by retaining up to second-order terms in the expansion of (35) as

$$\begin{aligned} c_{c+}(z) &= c_0 + c_0 \int \cdot \frac{g_{c\xi} g_{\xi c} [j\phi_{c\xi} z - \exp\{j\phi_{c\xi}(z-L)\} + \exp\{-j\phi_{c\xi} L\}]}{\phi_{c\xi}^2}\, d\xi \\ &= c_0 + c_0 \int \cdot \frac{\alpha_\xi [j\phi_{c\xi} z - \exp\{j\phi_{c\xi}(z-L)\} + \exp\{-j\phi_{c\xi} L\}]}{\phi_{c\xi}^2}\, d\beta_\xi \end{aligned} \tag{40}$$

where

$$\alpha_\xi = g_{c\xi} g_{\xi c} (\beta_\xi/\xi). \tag{41}$$

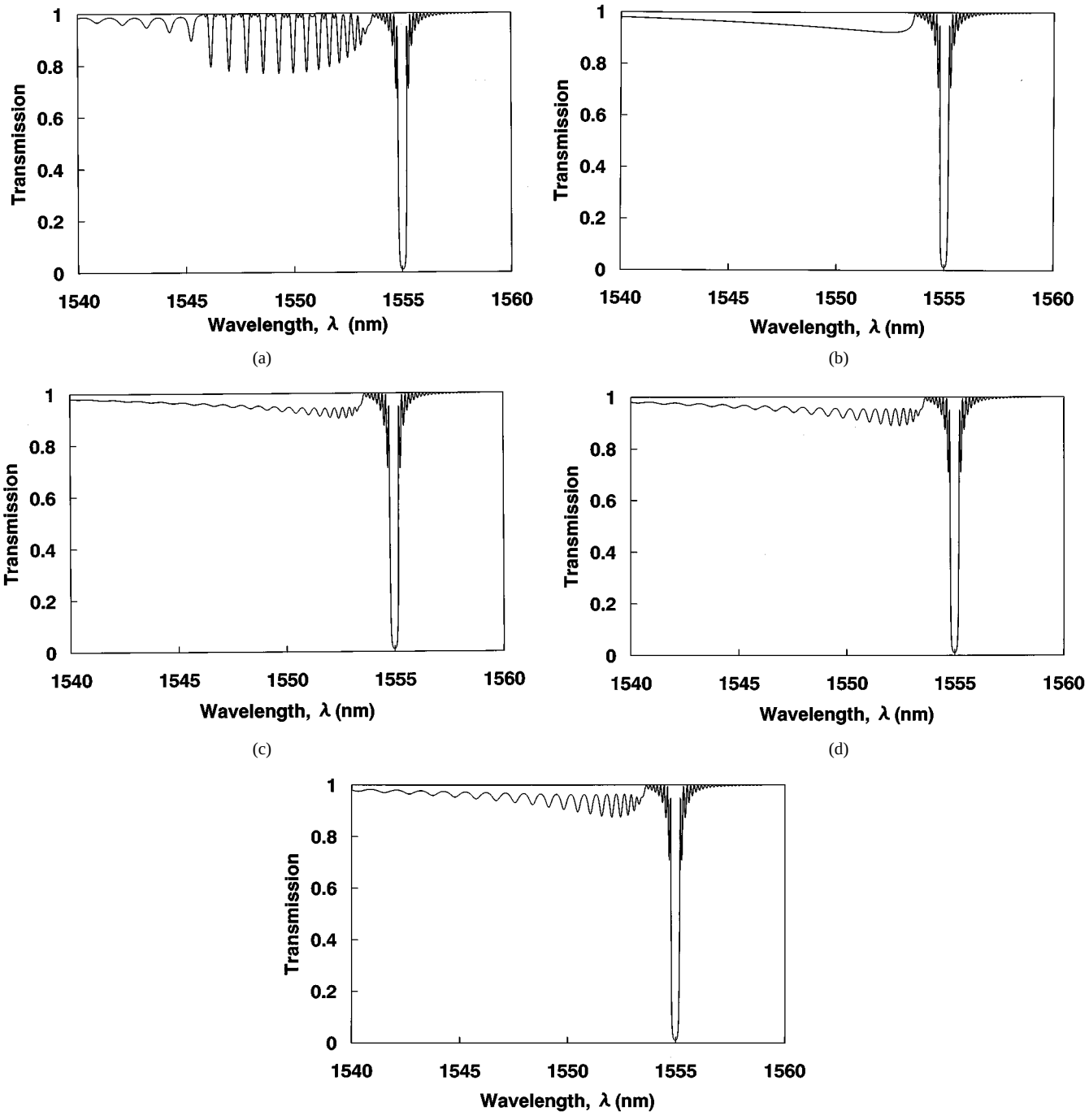

Fig. 4. Calculated transmission spectra through the FBGs with external indexes of: (a) $n_3 = 0.99n_2$, (b) $n_3 = n_2$, (c) $n_3 = 1.002n_2$. (d) $n_3 = 1.005n_2$, and (e) $n_3 = 1.01n_2$.

The amplitude transmission coefficient of the grating is given by

$$\frac{c_{c+}(L)}{c_0} = 1 + \int \frac{\alpha_\xi [j\phi_{c\xi} L - 1 + \exp\{-j\phi_{c\xi} L\}]}{\phi_{c\xi}^2} \, d\beta_\xi. \tag{42}$$

Equation (42) gives the true value of the transmission coefficient when the loss caused by the coupling to the radiation modes is small. When the loss is larger, it may be necessary to include higher order terms in the expansion of (35).

Most of the contribution to the integration of (42) comes from a narrow range of the propagation constant about $\beta_\xi = 2\pi/\Lambda - \beta_c$ that satisfies $\phi_{c\xi} = 0$. The factor α_ξ can be taken outside of the integral if it varies slowly with β_ξ. Fig. 3 shows the values of α_ξ as functions of β_ξ for FBGs surrounded with (a) index-matching material ($n_3 = n_2$) and (b) high index material ($n_3 = 1.01n_2$). It is seen that α_ξ varies slowly with β_ξ if $n_3 = n_2$, whereas it varies rapidly with β_ξ, exhibiting fringes with a large amplitude when $n_3 = 1.01n_2$. The fringes in Fig. 3(b) are because of the β_ξ-dependence of the field mag-

nitude in the surrounding material described in the previous section.

By referring to Fig. 3, we can take α_ξ outside of the integral when $n_3 = n_2$ and can accomplish the integration analytically, so that we finally obtain

$$\frac{c_{c+}(L)}{c_0} = 1 - \pi\alpha_\xi L \tag{43}$$

where the index ξ refers to a value where $\beta_\xi = 2\pi/\Lambda - \beta_c$. Equation (43) is valid only when $\pi\alpha_\xi L \ll 1$, but it can be modified in order to apply it to large $\pi\alpha_\xi L$ values by adding higher order terms in the expansion of (35)

$$\begin{aligned}\frac{c_{c+}(L)}{c_0} &= 1 - \pi\alpha_\xi L + \frac{1}{2}(\pi\alpha_\xi L)^2 - \frac{1}{3!}(\pi\alpha_\xi L)^3 + \cdots \\ &= \exp(-\pi\alpha_\xi L).\end{aligned} \tag{44}$$

From (44) we understand that the factor $\pi\alpha_\xi$ represents the amplitude loss coefficient within the grating, and it can be shown, after some manipulation, that the factor $\pi\alpha_\xi$ agrees with the corresponding factor in [4] that was derived for FBGs with infinite cladding radius.

When $n_3 \neq n_2$ and α_ξ varies rapidly with β_ξ as shown in Fig. 3(b), it cannot be taken outside the integral in (42), and, hence, the integration has to be carried out numerically.

Since the magnitude of Δn is as small as less than 10^{-3}, the field mismatch is negligible between LP_{01} modes with and without "dc" perturbation, i.e., within and outside the grating. Hence, we can regard $c_{c+}(0)$ and $c_{c+}(L)$ as the amplitude of incoming and outgoing LP_{01} modes to and from the FBG, respectively.

IV. Numerical Result

As an example of numerical calculation, we consider an FBG with a period of $\Lambda = 530$ nm, a length of $L = 0.5$ cm, a UV-induced index change of $\Delta n = 5 \times 10^{-4}$, and a fringe visibility of $m = 1$. The FBG is formed in a fiber with a core radius of $a = 2.3\,\mu$m, a cladding radius of $b = 62.5\,\mu$m, and a core-cladding index difference of $(n_1 - n_2)/n_1 = 0.007$. We calculated transmission spectra through the FBGs with external indexes of $n_3 = 0.99n_2$, $n_3 = n_2$, $n_3 = 1.002n_2$, $n_3 = 1.005n_2$, and $n_3 = 1.01n_2$. The results are shown in Fig. 4. The main Bragg band caused by the coupling between progressive and regressive LP_{01} modes is centered at a wavelength of $\lambda_0 = 1555$ nm. The series of loss bands on the short wavelength side of the main Bragg band in Fig. 4(b), (c), (d), and (e) are caused by the coupling of the LP_{01} mode to the radiation modes. With Fig. 4(a), the loss bands come from coupling to the cladding modes in the $\lambda > 1546$ nm wavelength range and to the radiation modes for $\lambda < 1546$ nm. We used (42) to calculate the extinction due to coupling to the radiation modes. We calculated the main Bragg dip and the remaining dips due to coupling to the cladding modes by applying conventional coupled mode theory.

In Fig. 4(a), where the index of the surrounding material is lower than that of the cladding ($n_3 = 0.99n_2$), the fiber supports 16 cladding modes to which the LP_{01} mode couples in the 1546 nm $< \lambda <$ 1554 nm wavelength range. Well-defined dips seen in that range correspond to the coupling to each of the cladding modes. The fringes in the $\lambda < 1546$ nm range are due to coupling to the radiation modes. Fig. 4(a) clearly shows that the fringes caused by the coupling to the radiation modes are more shallow than the dips caused by the coupling to the cladding modes. In Fig. 4(b), where the FBG is surrounded by index matching material ($n_3 = n_2$), we can see a smooth transmission profile in the wavelength range of $\lambda < 1554$ nm demonstrating the loss due to the coupling of LP_{01} mode to the continuum of radiation modes. In Fig. 4(c), (d), and (e), where the index of the surrounding material is higher than that of the cladding ($n_3 = 1.002n_2$, $1.005n_2$, $1.01n_2$), the transmission spectra now exhibit fringes. Such fringes in the transmission spectra have already been observed experimentally [2] but have not yet been theoretically estimated. The source of these fringes is the same as that of the fringes shown in Fig. 3(b) and is the Fabry–Perot-like interference resulting from the partial reflection of the radiated fields off the cladding-surrounding interface. A comparison of Fig. 4(c), (d), and (e) shows that the fringes become deeper as the cladding-surrounding index difference increases.

V. Conclusion

This paper presented an analysis of the coupling of the core mode to the radiation modes in FBGs with a finite cladding radius. We showed field distributions of the radiation modes, demonstrating that they are influenced significantly by the index mismatch between the cladding and the surrounding material even if the degree of mismatch is small. We derived a formula to calculate the core mode transmission loss caused by the radiation mode coupling. A closed-form formula for the amplitude loss coefficient of the core mode that we derived for FBGs surrounded by index-matching material agreed with a corresponding previously reported formula [4] that was derived for FBGs with infinite cladding radius. We showed calculated core mode transmission spectra that exhibited fringes like those already observed experimentally but yet to be estimated theoretically.

References

[1] "Special issue on fiber gratings, photosensitivity, and poling," *J. Lightwave Technol.*, vol. 15, pp. 1263–1512, Aug. 1997.
[2] T. Erdogan, "Fiber grating spectra," *J. Lightwave Technol.*, vol. 15, pp. 1277–1294, Aug. 1997.
[3] ——, "Cladding-mode resonances in short and long period fiber grating filters," *J. Opt. Soc. Amer. A*, vol. 14, pp. 1760–1773, Aug. 1997.
[4] V. Mizrahi and J. E. Sipe, "Optical properties of photosensitive fiber phase grating," *J. Lightwave Technol.*, vol. 11, pp. 1513–1517, Oct. 1993.
[5] T. Erdogan and J. E. Sipe, "Tilted fiber phase gratings," *J. Opt. Soc. Amer. A*, vol. 13, pp. 296–313, 1996.
[6] D. Marcuse, *Theory of Dielectric Optical Waveguides*, 2nd ed. New York, NY: Academic, 1991.

Yahei Koyamada (M'96), photograph and biography not available at the time of publication.